CrossMark

Theoretical Assessment on the Phase Transformation Kinetic Pathways of Multi-component Ti Alloys: Application to Ti-6Al-4V

Yanzhou Ji , Tae Wook Heo, Fan Zhang, and Long-Qing Chen

(Submitted September 14, 2015; in revised form November 19, 2015; published online December 21, 2015)

We present our theoretical assessment of the kinetic pathways during phase transformations of multi-component Ti alloys. Employing the graphical thermodynamic approach and an integrated free energy function based on the realistic thermodynamic database and assuming that a displacive structural transformation occurs much faster than long-range diffusional processes, we analyze the phase stabilities of Ti-6Al-4V (Ti-6wt.%Al-4wt.%V). Our systematic analyses predict a variety of possible kinetic pathways for β to (α + β) transformations leading to different types of microstructures under various heat treatment conditions. In addition, the possibility of unconventional kinetic pathways is discussed. We also briefly discuss the application of our approach to general multicomponent/multiphase alloy systems.

1. Introduction

A thorough understanding of the phase transformation mechanisms of Ti alloys is an important prerequisite for improving and controlling their mechanical properties. The microstructures of Ti alloys are sensitive to the transformation pathways that are determined by thermo-mechanical processing conditions and alloying chemistry. In particular, different cooling histories and compositions of β-stabilizers (e.g., β isomorphous elements: V, Mo, Nb, and β eutectoid-forming elements: Cr, Fe, Si) and/or α-stabilizers (e.g., substitutional element: Al, interstitial elements: O, N, C)[1,2] of multi-component Ti alloys result in a wide spectrum of two-phase (α + β) microstructures. For example, the β

Yanzhou Ji and **Long-Qing Chen,** Department of Materials Science and Engineering, The Pennsylvania State University, University Park, PA 16802, USA; **Tae Wook Heo,** Materials Science Division, Lawrence Livermore National Laboratory, Livermore, CA 94550, USA; and **Fan Zhang,** CompuTherm LLC, 437 S. Yellowstone Dr. Suite 217, Madison, WI 53719, USA. Contact e-mail: yxj135@psu.edu.

transus (T_β) of Ti-6Al-4V (Ti-6wt.%Al-4wt.%V) ($\sim 1000\ °C$[3]) is different from that of pure Ti ($\sim 882\ °C$[4]), and the alloying elements Al (α-stabilizer) and V (β-stabilizer) enhance the stabilities of α and β phases, respectively. As a result, Ti-6Al-4V alloys display dual-phase (α + β) microstructures over a wide temperature range. The continuous cooling from above T_β after hot deformation may result in a fully lamellar microstructure (or basket-weave and Widmanstätten microstructure). On the other hand, bi-modal microstructure (consisting of globular α grains and lamellar α plates) or fully equiaxed microstructure can be achieved depending on cooling rates if the alloy is cooled at a temperature below T_β along with hot plastic deformation in the (α + β) phase field. It should be noted that the features of phase microstructures such as the size of α colonies, the width of α lamellae, and the configuration of α grains directly influence the strength and ductility of the alloy.[2,5] These microstructural characters are mainly determined by the two major kinetic processes: β (*bcc*) to α (*hcp*) allotropic displacive transformation and long-range diffusion of alloying elements. Therefore, the understanding of kinetics of these two processes and their interplay is critically important for tailoring the phase microstructures and optimizing the mechanical behaviors of the alloys. A number of experimental studies[6-10] have been published in this regard. It has been shown that the compositional and structural (in)stabilities determine whether the diffusional phase transformation occurs through nucleation-and-growth or spinodal decomposition and whether the structural change occurs through discontinuous or continuous displacive transformations, respectively. For instance, in the case of Ti-6Al-4V, upon slow cooling (<20 K/s) from above T_β, α phase can precipitate in the β matrix through the diffusional nucleation-and-growth process,[11] whereas the β → α transformation takes place displacively without the compositional change under fast cooling (>20 K/s).[12] In addition, precipitation of Ti_3Al may occur during isothermal

aging at lower temperatures.[1] Note that it is challenging to precisely characterize these phase transformation mechanisms in experiments due to their complexity.

Theoretical investigations based on the so-called "graphical thermodynamic approach"[13] have established the systematic understanding of the complicated coupling of the kinetic processes during phase transformations in several alloy systems including Al-Li,[14] Ni-Al, Ni-Ti,[13] ZrO$_2$-Y$_2$O$_3$ alloys[15] and other generic systems.[16,17] They are mainly based on the analysis of relevant phase stabilities with respect to compositional and/or structural changes. Specifically for Ti alloys, the decomposition of β phase and the formation of ω phase have been graphically illustrated.[18,19] Recently, Heo et al.[20] applied the graphical thermodynamic approach to systematically analyzing the kinetic pathways in a model Ti-M binary alloy exhibiting two-phase (α + β) microstructures. They also explained the experimentally observed microstructures based on their proposed kinetic pathways of phase transformations. Boyne et al.[21] demonstrated the presence of the pseudospinodal mechanism[17] and Wang et al.[22] reported the precursory-spinodal mechanism in β-Ti alloys using computer simulations.

In this study, we extend the theoretical framework of Heo et al.[20] to multi-component Ti alloys. Employing a ternary Ti-6Al-4V alloy as a model system and its thermodynamic database, we systematically analyze the possible kinetic pathways under various heat treatment conditions.

2. General Framework: Graphical Thermodynamic Approach for Multi-component Alloys

The thermodynamic and kinetic characteristics of phase transformations of alloys can be analyzed by examining the variation of the Gibbs free energy (G) with respect to the change of thermodynamic configurations (e.g., composition, crystallographic structure, long-range or short-range ordering, etc.) under given temperature (T) and pressure (p). Mathematically, the state of a phase is represented by a point on the Gibbs free energy landscape (or hypersurface) as a function of configurational variables such as compositions (X) and order parameters (η). The possible pathways of a transformation from one phase state to another are directly related to their local topological features (i.e., phase stabilities) on the hypersurface. More specifically, the stability of a given phase and the features of phase transitions are determined by the following two major factors: (1) the local variational characteristics of G at the given point on the hypersurface with respect to infinitesimal perturbations of the thermodynamic configurations (i.e., the second derivatives of G with respect to configurational variables), which determines whether the given phase is stable or unstable; (2) the relative value of G itself on the phase transition pathway, which determines the relative (meta)stability of the given phase with respect to other phase states. Fundamentally, the most probable phase transformation pathway is the trajectory that has the minimum energy barriers on the Gibbs free energy hypersurface since the relevant kinetic processes are usually thermally activated

ones. Therefore, the phase stability analysis based on graphical examination (i.e., "graphical thermodynamic approach") of the Gibbs free energy hypersurface topology may provide the systematic understanding of the kinetic phase transformation pathways along minimal energy barrier trajectory.

The first step of the graphical thermodynamic approach is to construct a free energy function that can describe the relevant kinetic processes. Let us consider a general multi-component and multi-phase system under given T and p. The multiple compositions of the N alloying elements are expressed by $(X_1, X_2, \ldots, X_N)$. The structural changes from the parent phase to M product phases are represented by a set of order parameters $(\eta_1, \eta_2, \ldots, \eta_M)$. Based on these configurational variables, the total free energy of the system may be expressed as the following:[23,24]

$$
\begin{aligned}
f(\{X\}, \{\eta\}) = &\left(1 - \sum_{i=1}^{M} h(\eta_i)\right) \cdot f^0(\{X\}) \\
&+ \sum_{i=1}^{M} h(\eta_i) \cdot f^i(\{X\}) + g(\{\eta\}),
\end{aligned}
\tag{Eq 1}
$$

where $f^i(\{X\})(i = 0, 1, \ldots, M)$ are the molar Gibbs free energies of different phases, $h(\eta_i)$ is an interpolation function that relates the phases to the molar Gibbs free energy as a function of relevant compositions, and $g(\{\eta\})$ is a Landau-type free energy that describes the structural transformations. As shown in Fig. 1, we consider a phase transformation from a homogeneous parent phase (labeled as "0" in the figure) corresponding to $\left(\{X\}^0, \{0\}\right)$ to the final equilibrium state (labeled as "e") corresponding to $(\{X\}^e, \{\eta\}^e)$. Between these two states, we assume that there are two different intermediate metastable states (labeled as "A" and "B") corresponding to $\left(\{X\}^A, \{\eta\}^A\right)$ and $\left(\{X\}^B, \{\eta\}^B\right)$, respectively, on the possible $0 \rightarrow e$ transformation paths. Assuming that all these phase states are located at stationary points (i.e., $\left.\frac{\partial f}{\partial \eta_i}\right|_{\{\eta\}^s} = 0$), the relative stabilities of the different states are then determined by the above-mentioned two criteria. Specifically,

(1)   The positive-definiteness of the Hessian matrices

$$
\mathbf{H} = \left.\begin{pmatrix}
\frac{\partial^2 f}{\partial X_1^2} & \cdots & \frac{\partial^2 f}{\partial X_1 \partial X_N} & \frac{\partial^2 f}{\partial X_1 \partial \eta_1} & \cdots & \frac{\partial^2 f}{\partial X_1 \partial \eta_M} \\
\vdots & \ddots & \vdots & \vdots & \ddots & \vdots \\
\frac{\partial^2 f}{\partial X_N \partial X_1} & \cdots & \frac{\partial^2 f}{\partial X_N^2} & \frac{\partial^2 f}{\partial X_N \partial \eta_1} & \cdots & \frac{\partial^2 f}{\partial X_N \partial \eta_M} \\
\frac{\partial^2 f}{\partial \eta_1 \partial X_1} & \cdots & \frac{\partial^2 f}{\partial \eta_1 \partial X_N} & \frac{\partial^2 f}{\partial \eta_1^2} & \cdots & \frac{\partial^2 f}{\partial \eta_1 \partial \eta_M} \\
\vdots & \ddots & \vdots & \vdots & \ddots & \vdots \\
\frac{\partial^2 f}{\partial \eta_M \partial X_1} & \cdots & \frac{\partial^2 f}{\partial \eta_M \partial X_N} & \frac{\partial^2 f}{\partial \eta_M \partial \eta_1} & \cdots & \frac{\partial^2 f}{\partial \eta_M^2}
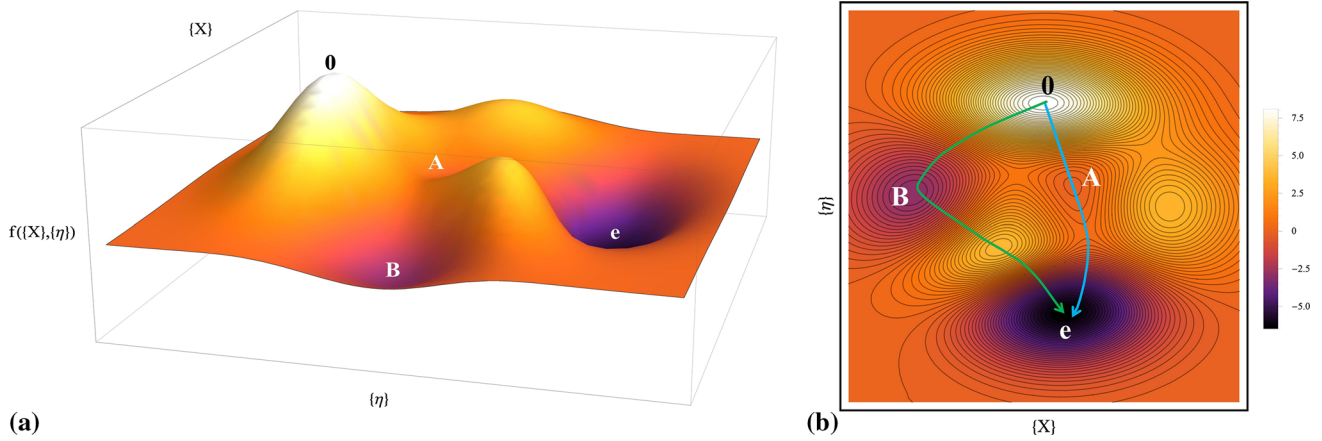\end{pmatrix}\right|_{(\{X\}^s, \{\eta\}^s)}
\tag{Eq 2}
$$

Fig. 1 (color online) (a) The illustration of a Gibbs free energy hypersurface on a X-η space. The state "0" represents the initial unstable state, the states "A" and "B" represent two metastable intermediate states, and the state "e" is the equilibrium state at given conditions. (b) Possible kinetic pathways 0 → A → e (the blue arrow on the right) and 0 → B → e (the green arrow on the left)

for given state s (s = 0, e, A, B). We note that, for the state s, the positive-definite, negative-definite, or indefinite Hessian matrix implies that a state is at local minimum, local maximum, or saddle point, respectively. When the given state is located at the local minimum, the state is stable with respect to small variations of both composition and structure. On the other hand, when the given state is located at the local maximum or saddle point, the state is unstable with respect to any compositional or structural variations depending on whether composition-related or order parameter-related eigenvalues of Eq 2, respectively, are negative. Note that the compositional instability and structural instability lead to spinodal decomposition and continuous displacive transformation (or continuous ordering), correspondingly.

(2) The relative values of the Gibbs free energy $(f(\{X\}^s, \{\eta\}^s))$ for the given state s (s = 0, e, A, B) on the possible pathways. According to criterion (1), the e, A and B states in Fig. 1 are all stable or metastable with respect to small perturbations of composition and order parameter. However, their values of Gibbs free energy are different. The state e is located at the global minimum, while the states A and B are located at the local minima of which Gibbs free energies are higher than the state e counterpart. In this case, the states A and B are considered metastable with respect to the state e, which means that there exists the driving force for the phase transformation from state A (or B) to the equilibrium state (e) with an energy barrier. The transformation from a metastable phase to a stable equilibrium phase, either by diffusional or diffusionless processes, takes place through a nucleation-and-growth mechanism that requires overcoming the energy barrier along the transformation pathway. In addition, the minimum energy barrier can be determined by finding the saddle points between the metastable state and the most stable (equilibrium) state.[25] For example, as illustrated in

Fig. 1(b), the lowest energy barriers for 0 → A → e and 0 → B → e pathways can be identified by finding the saddle points between A and e and between B and e, respectively. The 0 → A → e pathway is more likely to happen since it has lower energy barriers than the 0 → B → e pathway. It should be mentioned that additional factors should also be considered when the system contains other structural complexities such as grain boundaries, dislocations, etc. for analyzing the possible kinetic pathways.

3. Application to Ti-6Al-4V

We now apply the graphical thermodynamic framework to a particular alloy system. We choose Ti-6Al-4V as a model system of multicomponent Ti alloys. According to the existing thermodynamic assessment,[26,27] there exist three dominant phases (α (hcp), β (bcc) and Ti$_3$Al (DO$_{19}$)) in a microstructure of Ti-6Al-4V below T$_\beta$. The Gibbs free energy function of the system based on Eq 1 is formulated as:

$$f(X_{Al}, X_V, \eta, \phi, T) = (1 - h(\eta) - h(\phi)) \cdot f^\beta(X_{Al}, X_V, T)$$
$$+ h(\eta) \cdot f^\alpha(X_{Al}, X_V, T)$$
$$+ h(\phi) \cdot f^{Ti_3Al}(X_{Al}, X_V, T) + g(\eta, \phi)$$

(Eq 3)

where X_{Al} and X_V are the compositions of Al and V, respectively, η is the structural order parameter describing the bcc to hcp crystallographic structural change by the combined shear deformation and atomic shuffle based on the Burgers mechanism,[28] φ is the long-range order parameter for the ordered DO$_{19}$ structure, and $g(\eta, \phi)$ is a Landau-type free energy for structure transformations to α and DO$_{19}$ phases. For the interpolation function, we chose $h(x) = 3x^2 - 2x^3$, which is a simple possible form of h(x)

that ensures the local extremes of the parent phase ($x = 0$) and product phase ($x = 1$), and can capture the transition of parent phase stability with temperature change. We emphasize that the molar Gibbs free energies of β and α phase (f^β and f^α, respectively) are directly taken from the thermodynamic database,[26,27] which is valid over the entire composition ranges at $T > 300$ K. We analyze the β → (α + β) or β → (α + β + Ti$_3$Al) transformation pathways starting from the homogeneous β phase with initial compositions $(X_{Al}^0, X_V^0) = (0.1019, 0.036)$ in atomic fraction that corresponds to 6wt.% Al and 4wt.%V based on the criteria in section 2. We consider both isothermal and non-isothermal conditions in the following sections. It should be noted that the product α phase can be classified into the diffusional product α$_p$, the massive product α$_m$, and the martensitic product α' depending on associated kinetic processes, which are determined by cooling rate and chemical compositions. To avoid the complexity, we describe the free energies of these phases using the unified free energy function f^α with different compositions since the crystal structure of all these phases is *hcp* in common.

3.1 Isothermal Transformation Pathways

Under the isothermal condition, the Landau-type free energy in Eq 3 for a fixed temperature can be simply formulated as

$$g(\eta, \phi) = w^\alpha \cdot \eta^2(\eta - 1)^2 + w^{Ti_3Al} \cdot \phi^2(\phi - 1)^2 + \gamma \cdot \eta^2\phi^2$$
(Eq 4)

in a way that $(\eta, \phi) = (0, 0)$, $(1, 0)$ and $(0, 1)$ corresponds to the parent β phase, the α phase, the Ti$_3$Al phase, respectively. Accordingly, the energy humps w^α, w^{Ti_3Al} and γ across the α/β, β/Ti$_3$Al and α/Ti$_3$Al interfaces, respectively, are determined by interface properties based on the diffuse-interface description.[29] For nucleation and growth, the nucleation barrier is also expected to be proportional to the square root of this energy barrier determined from the molar Gibbs free energy function, according to the diffuse-interface theory.

By analyzing Eq 3 and 4, we identify the possible kinetic sequences of phase transformations from β to (α + β) phases at different isothermal aging temperatures. The entire temperature range is divided into several different regimes depending on the operating transformation mechanisms in terms of fundamental solvus or transus temperatures of relevant phases (e.g., the transus temperature of the β phase $(T_\beta) \sim 1249$ K (976 °C) and the solvus temperature of Ti$_3$Al ~ 895 K (622 °C) by our thermodynamic calculations). Each transformation pathway is determined by the coupling and/or competition of the following two major stabilities of given phases.

3.1.1 Phase Stabilities with Respect to Compositional Change. By evaluating the compositional part of the Hessian matrix in Eq 2:

$$\mathbf{H^c} = \begin{pmatrix} \frac{\partial^2 f}{\partial X_{Al}^2} & \frac{\partial^2 f}{\partial X_{Al}\partial X_V} \\ \frac{\partial^2 f}{\partial X_V\partial X_{Al}} & \frac{\partial^2 f}{\partial X_V^2} \end{pmatrix}$$
(Eq 5)

at $(X_{Al}, X_V, \eta, \phi) = (X_{Al}, X_V, 0, 0)$ at different temperatures, we may construct the phase stability map in the compositional space as shown in Fig. 2(a). The critical compositional boundaries across which the phase stability varies can
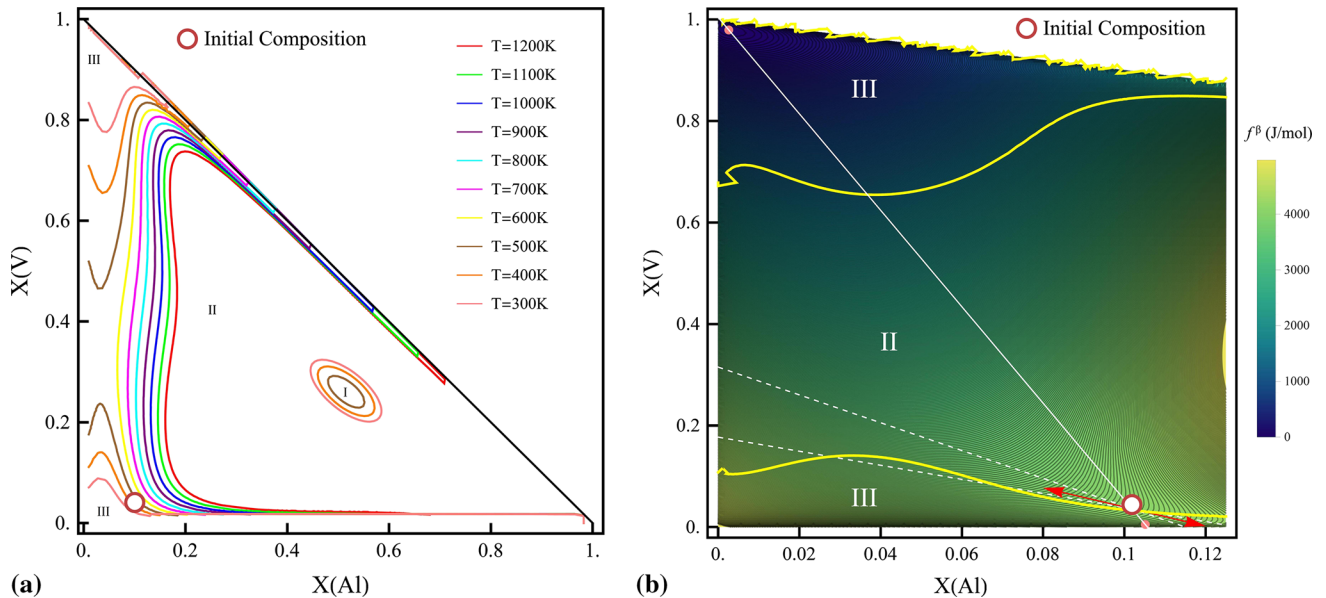

Fig. 2 (color online) Compositional stability analysis for β phase in Ti-Al-V system, using thermodynamic database functions. (a) Isothermal section of compositional instability surface at different temperatures. (b) Compositional stability analysis at $T = 400$ K for the initial composition of Ti-6Al-4V; the two pink points, linked by the white tie line, represent the equilibrium composition of β phase (upper left) and α phase (lower right), respectively; the thick yellow line separates stability region II and III; the two white dashed lines gives the compositional instability directions for β phase with the initial composition; the red arrows show the most unstable direction

be obtained by determining the critical compositions resulting in the indefinite Hessian matrix (i.e., its determinant equals zero). As shown in Fig. 2(a), the entire possible compositional space (satisfying $X_{Al} + X_V < 1$) is divided into three distinct regions[30] depending on signs of the determinant and eigenvalues of $\mathbf{H^c}$ as the following:

- *Region I* ($\mathbf{H^c}$ is negative-definite): β phase is unstable against compositional variations along all compositional directions;
- *Region II* ($\mathbf{H^c}$ has one positive and one negative eigenvalues): β phase is unstable against compositional variations along only specific compositional directions;
- *Region III* ($\mathbf{H^c}$ is positive-definite): β phase is stable for all compositional directions.

Here, the "compositional direction" refers to a variational direction of two-dimensional composition vector (X_{Al}, X_V) on the compositional space where the Gibbs free energy hypersurface is defined. For example, since the initial composition $(X_{Al}^0, X_V^0) = (0.1019, 0.036)$ of Ti-6Al-4V is always located within the instability regime below $T_s = 423.7$ K (~150.5 °C) as marked in Fig. 2(a), the β phase separation can occur through the spinodal decomposition into solute-rich (β₁) and solute-lean (β₂) phases maintaining *bcc* structures without having to overcome a phase nucleation barrier. The decomposed phases may then undergo complicated transformation sequences to reach the most stable (α + β + Ti₃Al) mixture with the corresponding equilibrium compositions. Detailed information regarding the kinetic pathways can be extracted by closely examining the Hessian matrix. For instance, for the same compositions at $T = 400$ K, although both diagonal terms ($\frac{\partial^2 f}{\partial X_{Al}^2}$ and $\frac{\partial^2 f}{\partial X_V^2}$) of $\mathbf{H^c}$ are positive, one of the eigenvalues of $\mathbf{H^c}$ becomes negative. In this case, the unstable compositional directions can be calculated by

$$(\mathbf{H^c v}) \cdot \mathbf{v} \le 0 \qquad\qquad \text{(Eq 6)}$$

where $\mathbf{v} = (\cos\theta, \sin\theta)^T$ is a directional unit vector of compositional variation from the initial composition $(X_{Al}^0, X_V^0) = (0.1019, 0.036)$ with an angle θ. Based on Eq 6, we find that the unstable compositional directions lie between the two white dashed lines in Fig. 2(b). In addition, the most probable decomposition direction can be determined by finding the unit vector $\mathbf{v}$ that results in the largest compositional instability, (i.e., the most negative value of $(\mathbf{H^c v}) \cdot \mathbf{v}$), or alternatively, by finding the eigenvector of $\mathbf{H^c}$ that corresponds to the negative eigenvalue of $\mathbf{H^c}$. This direction is indicated by the red arrows in Fig. 2(b). We note here that there are possible structural instabilities during the compositional change within this regime as discussed later. In fact, the experimental observation of the β to (β₁ + β₂) decomposition is rare due to the difficulty of retaining β phase at low temperatures with the composition of β-stabilizer in Ti-6Al-4V. In practice, the decomposition of β solid solution usually takes place in β-Ti alloys with more content of β-stabilizers[2] even though there exists the theoretical possibility of the spinodal decomposition in Ti-6Al-4V.

Above the critical temperature T_s for spinodal decomposition, the compositional instability vanishes. Therefore, the transformation pathway is determined by the relative stabilities of possible phases within this regime. Since the relative stabilities of metastable phases are determined by the relative values of the Gibbs free energy according to criterion (2) in section 2, the critical temperature across which the relative phase stability varies is simply determined by finding the temperature at which the Gibbs free energies of the associated two phases are equal: $f^\beta(X_{Al}^0, X_V^0, T) = f^\alpha(X_{Al}^0, X_V^0, T)$. For a homogeneous β phase of Ti-6Al-4V with the composition $(X_{Al}^0, X_V^0) = (0.1019, 0.036)$, the critical temperature T_0 for α and β phases is ~1145 K (872 °C) according to our calculation based on the thermodynamic database. Note that this critical temperature is lower than the β transus, which means that it is still within the two-phase (α + β) regime. This means α phase, with a composition that is different from the nominal composition, may directly nucleate and grow from β phase below the β transus and above the critical temperature (1145 K), leading to the equilibrium two-phase (α + β) microstructure, as illustrated in Fig. 3(a). On the other hand, below the critical temperature, the *bcc* (β) to *hcp* (α) structural transformation may first take place through diffusionless displacive transformation via the nucleation-and-growth mechanism due to the metastability of the β phase followed by the diffusional α → (α + β) transformation through the nucleation-and-growth mechanism due to the metastability of the α phase, as illustrated in Fig. 3(b). Although there is a possibility of direct nucleation of α phases from the initial β phase resulting in the two-phase microstructure (i.e., β → α + β) as the case above the critical temperature, the diffusionless β → α transformation is more likely to occur prior to the formation of the final two-phase microstructure. This is because the structural change involves local atomic movements (e.g., shear and shuffle) or short-range diffusion (e.g., massive transformation[12]) regardless of the metastability of the initial β phase, which are usually much faster than the long-range diffusional processes. Therefore, the pathway β → α → (α + β) is most probable within this regime.

For the temperatures close to T_β above the critical temperature, the driving force for phase transformation is quite small. According to the classical nucleation theory,[31] the small driving force leads to high nucleation barrier and large critical nucleus size, which results in the lower nucleation probability. Therefore, homogeneous nucleation events of the α phase from the initial β grains rarely occur. In this case, the α phase may heterogeneously nucleate at or near β grain boundaries (GBs) and/or dislocations inside β grains,[32] which requires the significantly lower nucleation barrier. As the temperature decreases, the homogeneous nucleation of the α phase inside the grains becomes more competitive with respect to heterogeneous nucleation. These microstructural features have been experimentally observed in Ti-6Al-4V under isothermal conditions.[33]

The thermodynamic database indicates that DO_{19}-ordered Ti_3Al precipitates may appear below 895 K. The formation of Ti_3Al precipitates in Ti alloys has been experimentally reported[34] especially when the oxygen concentration is relatively high (~0.2 wt.%). The Ti_3Al phase has been also theoretically investigated in terms of statistical thermodynamics and ordering kinetics.[35] To consider the phase stability of Ti_3Al, we formulated f^{Ti_3Al} as a function of explicit compositions based on the sublattice model $(Ti,Al,V)_3$ (Ti,Al,V) for the Ti-Al-V ternary database.[26,27] Employing the criterion (2) in section 2, the possible kinetic pathway of phase transformations is identified to be diffusional $\alpha \rightarrow (\alpha + \beta + Ti_3Al)$ through the nucleation-and-growth mechanism after the diffusionless displacive $\beta \rightarrow \alpha$ transformation, as illustrated in Fig. 3(c), or diffusional $\beta \rightarrow (\alpha + \beta + Ti_3Al)$ through the nucleation-and-growth mechanism.
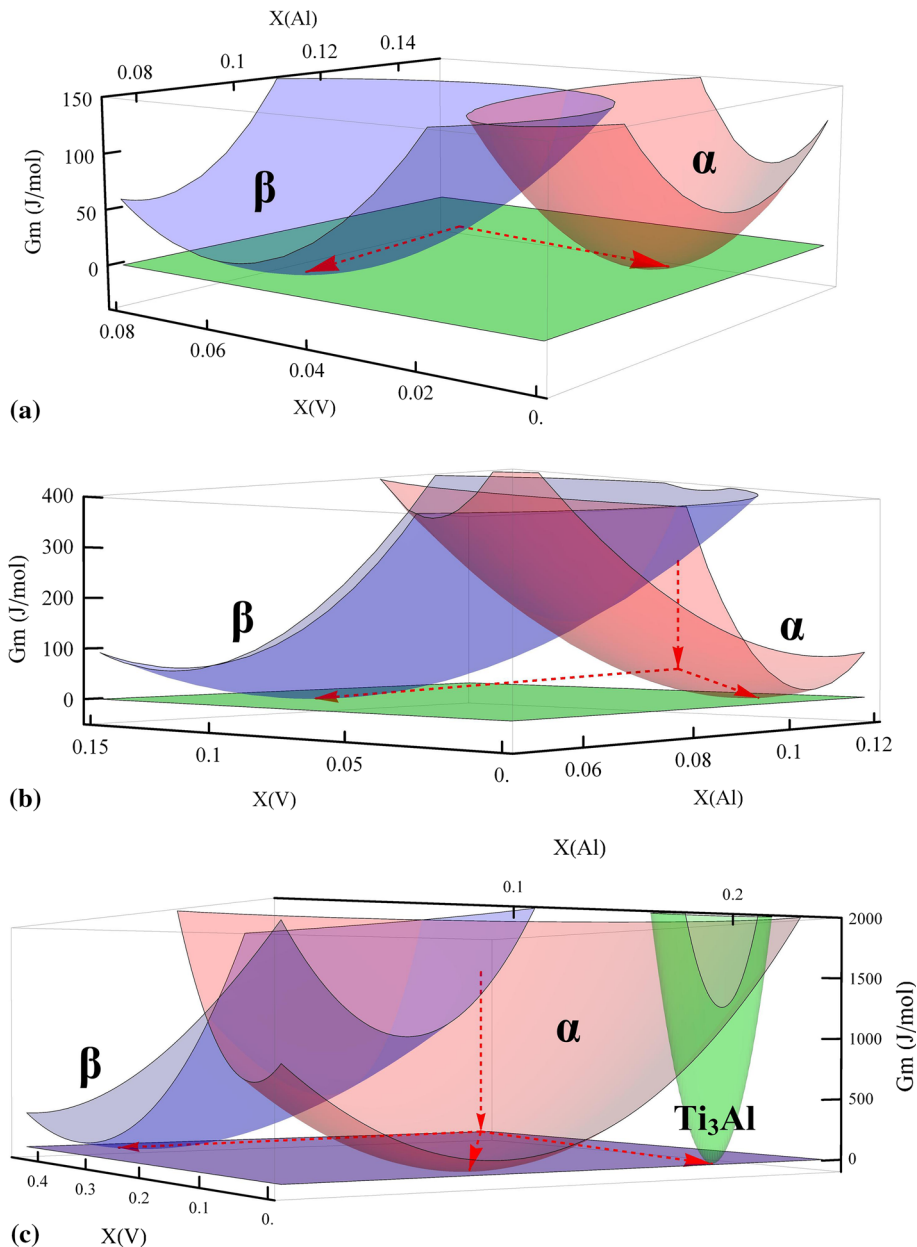

Fig. 3 (color online) The illustration of kinetic pathways in Ti-6Al-4V under isothermal condition for (a) T_0 (1145 K) $< T < T_\beta$ (1249 K): $\boldsymbol{\beta} \rightarrow$ (*diffusional nucleation and growth*) $\rightarrow (\boldsymbol{\alpha + \beta})$; (b) T_{Ti_3Al} (895 K) $< T < T_0$ (1145 K): $\boldsymbol{\beta} \rightarrow$ (*diffusionless nucleation and growth*) $\rightarrow \boldsymbol{\alpha} \rightarrow$ (*diffusional nucleation and growth*) $\rightarrow (\boldsymbol{\alpha + \beta})$; (c) T_s (423 K) $< T < T_{Ti_3Al}$ (895 K): $\boldsymbol{\beta} \rightarrow$ (*diffusionless nucleation and growth*) $\rightarrow \boldsymbol{\alpha} \rightarrow$ (*diffusional nucleation and growth*) $\rightarrow (\boldsymbol{\alpha + \beta + Ti_3Al})$. The kinetic pathways start from a homogeneous β phase of Ti-6Al-4V with the composition $(X^0_{Al}, X^0_V) = (0.1019, 0.036)$. The dashed red arrow represents discontinuous transformations (through nucleation-and-growth mechanism). The bottom planes represent the common tangent planes of the molar Gibbs free energies of the phases presented

3.1.2 Phase Stabilities with Respect to Structural Change. According to theoretical studies on phonon dispersion curves of pure Ti,[36,37] the β phase becomes dynamically unstable ($\frac{\partial^2 f}{\partial \eta^2} \leq 0$) at low temperatures (e.g., below $T_c = 484.4$ K in[37]), since the shear modulus ((C_{11}-C_{12})/2) becomes negative and the energy barrier for the transformation to α phase vanishes. Within this regime, the *bcc* to *hcp* displacive transformation would occur continuously. On the other hand, above T_c, the displacive transformation discontinuously takes place through a nucleation-and-growth mechanism (i.e., martensitic transformation) due to the metastability ($\frac{\partial^2 f}{\partial \eta^2} > 0$) of the β phase. The M_s temperature reflects a critical (or minimum) driving force for the β → α (or α') martensitic transformation to take place. From the available TTT diagrams of Ti-6Al-4V, we know that discontinuous (martensitic) displacive transformations can take place during isothermal heating at or near martensite start transformation temperature (M_s) (around 550-650 °C),[1,38-40] which is an example of the β → α → (α + β) pathway discussed in section 3.1.1. In this study, since the martensitic phase α' in Ti-6Al-4V also has the *hcp* structure but differs with the diffusional α products in compositions, we use the same thermodynamic function $f^\alpha(X_{Al}, X_V, T)$ to describe α' and the diffusional α products rather than treating the metastable α' as another phase.

Assuming $M_s = 873$ K (600 °C), then this critical driving force can be estimated to be 1200 J/mol by $\Delta G = f^\beta(X_{Al}^0, X_V^0, M_s) - f^\alpha(X_{Al}^0, X_V^0, M_s)$. By definition, the instability temperature T_c might be lower than M_s ($T_c < M_s$) for Ti-6Al-4V, which enables the estimation of w^α ($w^\alpha \geq 3602$ J/mol). It should be noted that the value of w^α depends on the choice of the interpolation function $h(\eta)$. Under the conditions: $\frac{\partial^2 h}{\partial \eta^2}\big|_{\eta=0} > 0$ and $\frac{\partial^2 h}{\partial \eta^2}\big|_{\eta=1} < 0$, w^α can be estimated in the same way for the given interpolation function. However, the major consequence of the kinetic pathway analysis will not change. The relative stabilities of *bcc* (β) and *hcp* (α) structures at various temperatures are

illustrated in Fig. 4(a). Note that β phase is still metastable with respect to the structural order parameter η at M_s; the free energy curve in Fig. 4(a) becomes concave at η = 0 when $T < T_c$.

Therefore, at temperatures below M_s, the system first undergoes discontinuous ($T_c < T < M_s$) or continuous ($T < T_c$) displacive β → α' transformation to form metastable α' martensites. Further decomposition into equilibrium (α + β + Ti$_3$Al) mixture by diffusional processes then occurs. However, the diffusional processes are often sluggish at such low temperatures in practice. For example, the metastable martensite structure is usually retained under room temperature in spite of the existence of driving forces for the diffusional transformations. The kinetic pathway is similar to that shown in Fig. 3(c). Note that we only focus on the temperature-dependence of the structural instabilities ignoring the possible contributions of finite deformation strains and shuffling amplitudes in the Landau-type free energy for simplicity. A more physical and complete Landau-type free energy for the β → α transformation will be discussed in our subsequent work.

Considering both compositional and structural (in)stabilities, we could systematically identify all possible kinetic pathways from a homogeneous β phase under the isothermal condition for different temperature ranges as tabulated in Table 1. Since it is difficult to determine the critical temperature T_c in Ti-6Al-4V, we ignore the temperature regime for the continuous displacive transformation in Table 1.

3.2 Non-isothermal Transformation Pathways During Cooling

To control the microstructures for optimizing their mechanical properties, Ti alloys are usually treated by continuous cooling processes from above T_β. Compared to the isothermal condition discussed in section 3.1, the most significant difference in rapidly cooled Ti alloys is the higher possibility of displacive transformations due to the larger transformation driving forces during cooling. To account for the effect of undercooling on the thermody-
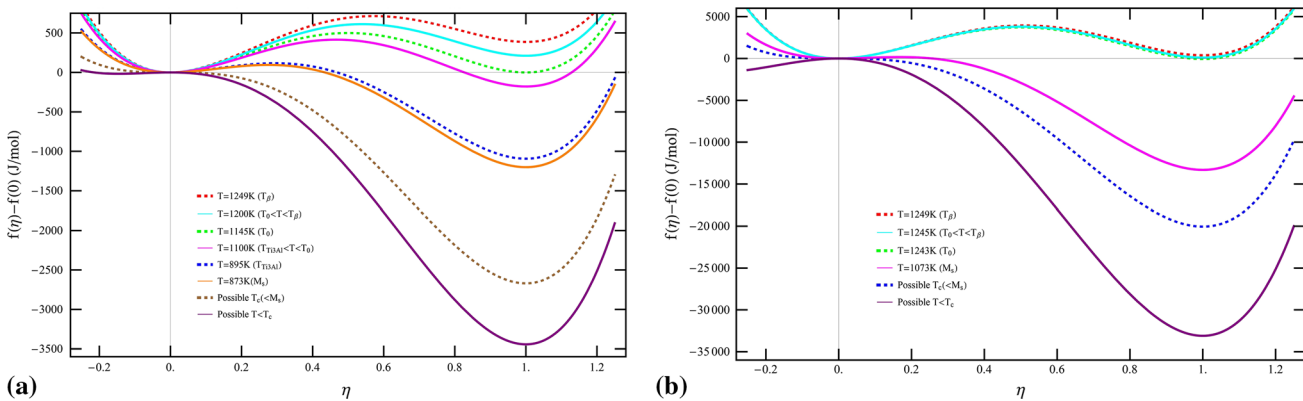

Fig. 4 (color online) Stability of β phase with respect to structure change at various temperatures. (a) Isothermal case; (b) rapid cooling (or high undercooling). β phase is at η = 0 and α phase is at η = 1. At $T = M_s$, β phase (η = 0) is still metastable with respect to β → α structure change

Table 1 Summary of kinetic pathways in Ti-6Al-4V under isothermal condition

Temperature range	Kinetic pathways
T_0 (1145 K) $< T < T_\beta$ (1249 K)	$\beta \rightarrow$ (*diffusional nucleation and growth*) $\rightarrow$ ($\alpha + \beta$)
T_{Ti_3Al} (895 K) $< T < T_0$ (1145 K)	$\beta \rightarrow$ (*diffusionless nucleation and growth*) $\rightarrow \alpha \rightarrow$ (*diffusional nucleation and growth*) $\rightarrow$ ($\alpha + \beta$)
T_s (423 K) $< T < T_{Ti_3Al}$ (895 K)	$\beta \rightarrow$ (*diffusionless, discontinuous*) $\rightarrow \alpha$ **or** α' (*martensite*) $\rightarrow$ (*diffusional nucleation and growth*) $\rightarrow$ ($\alpha + \beta + Ti_3Al$)
$T < T_s$ (423 K)	Competition between spinodal decomposition and martensitic transformation (or continuous displacive transformation)

namics of $\beta \rightarrow \alpha$ transformation in the free energy function, we formulate the Landau-type energy function as:

$$g(\eta, \phi, T) = w^\alpha \cdot \eta^2 (\eta - 1)^2 + \left(f^\beta(X_{Al}^0, X_V^0, T^0) - f^\beta(X_{Al}^0, X_V^0, T) \right) \cdot h(\eta) + w^{Ti_3Al} \cdot \phi^2 (\phi - 1)^2 + \gamma \cdot \eta^2 \phi^2$$

$$(Eq\ 7)$$

The additional term $\left(f^\beta(X_{Al}^0, X_V^0, T^0) - f^\beta(X_{Al}^0, X_V^0, T) \right) \cdot h(\eta)$ accounts for the contribution of the under-cooling. Due to the mathematical properties of the interpolation function $h(\eta) = 3\eta^2 - 2\eta^3$, the second derivative of $g(\eta, \phi, T)$ with respect to η can even become negative at low temperatures at $(\eta, \phi) = (0, 0)$ (i.e., the initial state can be structurally unstable) by choosing proper magnitudes of w^α, T^0 and T. In the case of Ti-6Al-4V, for the fast cooling rates (> 20 K/s), the diffusionless displacive transformation can take place. Upon cooling, the M_s temperature is usually higher than the isothermal counterpart. For example, M_s can reach $\sim 800\ °C$ under cooling according to existing experimental observations and CCT diagrams of the Ti alloy.[1,41,42] Again, we assume that M_s indicates a critical driving force to initiate the martensitic transformation. By setting $T^0 = T_\beta$, the driving force can be estimated to be 13,306 J/mol, which is higher than that of the isothermal case. This is because β phase becomes more stable as temperature increases, which requires larger driving force to initiate the $\beta \rightarrow \alpha'$ martensitic transformation. In addition, when the β phase becomes dynamically unstable under certain temperature T_c, i.e., $\left. \frac{\partial^2 f}{\partial \eta^2} \right|_{(X_{Al}, X_V, \eta, \phi, T) = (X_{Al}^0, X_V^0, 0, 0, T_c)} \leq 0$, the value of w^α should be larger than 39,917 J/mol since $T_c < M_s$. The β phase stability with respect to structural change for several temperatures is illustrated in Fig. 4(b).

The criteria in section 2 are also applicable to analyzing the kinetic pathways during cooling. First of all, for slow cooling (e.g. < 0.1 K/s), the temperature homogenization is allowed, resulting in small undercooling (T^0 is close to T). In this case, the phase transformation kinetic pathways are quite similar to those under the isothermal condition. During cooling, the α plates sequentially appear from GBs to grain interiors due to the change of nucleation modes, as discussed in section 3.1. In contrast, for fast cooling (> 20 K/s), the temperature homogenization of the sample is largely inhibited, resulting in large undercooling (T^0 is close to T_β). In this case, the diffusionless displacive

structural transformation can be dominant over the diffusional transformation due to the large driving force for initiating martensitic transformations. For example, assuming that $T^0 = T_\beta$, the critical temperature T_0 where the Gibbs free energies of the two phases are equal is shifted to 1243 from 1145 K of the isothermal case. Below this temperature, the diffusionless displacive transformation can happen through the nucleation-and-growth process. Moreover, the martensitic transformation can occur below M_s. It should be noted that the phases produced by the iso-compositional transformations, usually massive α or martensitic α, are thermodynamically metastable. Therefore, these phases can be further transformed to the equilibrium ($\alpha + \beta$) microstructures through the diffusional nucleation-and-growth process. However, due to the fast cooling, the temperature rapidly reaches to significantly low temperatures that may suppress the diffusional processes. As a result, the metastable phases can be retained for a long time ($\sim$years) at such low temperatures. For the case of intermediate cooling, the transformation pathways are influenced by more complicated competitions between diffusional and diffusionless processes. Depending on the cooling rate (or undercooling), the critical temperatures (T_0 and M_s) are expected to be shifted. With the increase of cooling rate (or undercooling), it is expected that the driving force for phase transformation of α phase may significantly increase, resulting in the increase of nucleation probability in grain interiors. Consequently, the width of α lamellae may decrease due to high nucleation density, which has been observed and discussed in several experimental investigations.[1,12,41]

The identified possible kinetic pathways of phase transformations with large undercooling are summarized in Table 2 based on our discussion above.

3.3 Generalization to Multi-component Ti Alloys

Commercial Ti alloys generally consist of multiple alloying elements and multiple phases. Even in the practically used Ti-6Al-4V, some minor alloying elements such as Fe, O, N, C and H are incorporated, which can influence the thermodynamic properties and kinetic transformation pathways of the alloy. For example, the addition of hydrogen can decrease both T_β and M_s, and change the crystal structure of martensite from hexagonal (α') to orthorhombic (α'').[43] Recently, the CALPHAD approach[44] has been extensively utilized to establish the thermodynamic descriptions for these multi-component and multi-phase Ti alloys.

Table 2 Summary of kinetic pathways in Ti-6Al-4V under rapid cooling (or high undercooling)

Temperature range	Kinetic pathways
T_0 (1243 K) $< T < T_\beta$ (1249 K)	$\beta \rightarrow$ (*diffusional nucleation and growth*) $\rightarrow$ ($\alpha + \beta$)
$T_{\mathrm{Ti_3Al}}$ (895 K) $< T < T_0$ (1243 K)	$\beta \rightarrow$ (*diffusionless nucleation and growth*) $\rightarrow$ α **or** α' (*martensite*) $\rightarrow$ (*diffusional nucleation and growth*) $\rightarrow$ ($\alpha + \beta$)
$T < T_{\mathrm{Ti_3Al}}$ (895 K)	$\beta \rightarrow$ (*diffusionless, discontinuous*) $\rightarrow$ α' (*martensite*) $\rightarrow$ (*diffusional nucleation and growth*) $\rightarrow$ ($\alpha + \beta + \mathrm{Ti_3Al}$)

Examples include several ternary,[45-48] quarternary,[49,50] pseudo-ternary[27] alloys, and several commercial multi-component Ti alloys. To account for the effects of the multiple alloying elements, these available thermodynamic databases can be employed to construct the Gibbs free energy functions for analyzing the phase stabilities. One simple example is to use the Ti-Al$_x$-V$_y$ pseudo-ternary database proposed by Zhang et al.[27] for alloys containing multiple α- and β-stabilizers, where Al$_x$ and V$_y$ represent the weighted summations of all α-stabilizers and β-stabilizers, respectively (i.e., Al$_x$ and V$_y$ represent the hypothetical Al and V, respectively, that embody the effects of all other α- and β-stabilizers). For instance, let us consider the following multi-component Ti alloy: Ti-6.624Al-4.096V-0.194Fe-0.1855O-0.0065N-0.02C-0.0044H in wt.% (or Ti-11.14Al-3.65V-0.1576Fe-0.5262O-0.0211N-0.0756C-0.1981H in at.%). According to the pseudo-ternary model, the given alloy is reduced to Ti-7.1275Al$_x$-4.497V$_y$ in wt.% (or Ti-12.017Al$_x$-4.016V$_y$ in at.%). The complex multi-component alloy is then treated as a ternary alloy. Therefore, the possible kinetic pathways can be analyzed using the same procedures as discussed in section 3.1 and 3.2 using the pseudo-ternary database for the given alloy. The main differences from Ti-6Al-4V are the change of critical temperatures (T_β (1233 K) and T_0 (1153 K)). Note that the change of M_s cannot be directly predicted from the pseudo-ternary database.

It should be mentioned that more accurate predictions for multi-component Ti alloys in terms of not only the changes of characteristic critical temperatures (T_β, T_0 and M_s, etc.), but also the formation of distinct minor phases (e.g., Laves phase, TiH$_2$, TiM_B2, etc.) can be established by directly employing the multi-component database. At the same time, the better accuracy of the multi-component Ti alloy database requires the more extensive experimental investigations and thermodynamic modeling using existing binary and ternary databases. However, we emphasize that the general procedures described in this work could also be applied to the multi-component systems.

4. Possible Extension to Non-conventional Kinetic Pathways in Ti-6Al-4V

In section 3, we mainly focus on the conventional kinetic pathways in bulk Ti-6Al-4V. In reality, there can be other possible non-conventional kinetic pathways due to the complexities and inhomogeneities of the alloys. In this section, we briefly discuss the relevant non-conventional pathways in connection to our current framework, the limitations of the current framework and the possible extensions.

4.1 Pseudospinodal Mechanism

The pseudospinodal mechanism[17] is one of non-classical transformation mechanisms that may become active near the critical temperature at which the Gibbs free energies of the two phases are identical for the given compositions. For example, the critical temperature is ~1145K for Ti-6Al-4V as discussed in section 3.1. The pseudospinodal mechanism is initiated by a partitionless or congruent $\beta \rightarrow \alpha$ transformation followed by decomposition, in which the compositions of the two phases continuously change towards equilibrium values, just like that in real spinodal decompositions.[6,21] However, unlike true spinodal decomposition, the two phases are of different symmetries and the pseudospinodal decomposition process may not necessarily be related to compositional instabilities. The mechanism was firstly proposed for explaining the cubic-to-tetragonal transformation,[17] and it was applied to analyzing the phase transformation mechanisms in a β-Ti alloy.[21] The key interesting microstructural features of the pseudospinodal mechanism in the Ti alloys are the sudden increase in the nucleation rate of α phase, leading to the development of fine α plates as the temperature approaches T_0.[6,21] Boyne[21] investigated the pseudospinodal mechanism in Ti-alloys by employing the phase-field simulations. The proposed transformation kinetic pathways in the pseudospinodal mechanism,[17] as well as the unexpected increase of the nucleation rate of α phase,[6] were well reproduced. We note that this mechanism lies between the mechanisms "$\beta \rightarrow$ (*diffusional nucleation and growth*) $\rightarrow$ ($\alpha + \beta$)" and "$\beta \rightarrow$ (*diffusionless nucleation and growth*) $\rightarrow$ $\alpha \rightarrow$ (*diffusional nucleation and growth*) $\rightarrow$ ($\alpha + \beta$)" in Table 1 as discussed in section 3.1.

4.2 Possible Pathways Due to the Structural Inhomogeneities in the System

The presence of structural inhomogeneities such as grain boundaries and dislocations often alters the transformation pathways since it perturbs the relevant chemical and/or elastic strain energetics in alloys. It may cause spatially inhomogeneous distribution of alloying elements, which gives rise to the local variation of phase stabilities. For example, grain boundaries often induce solute segregation/depletion to reduce the excess free energy (or grain

boundary energy). As a result, the compositions of alloying elements at or near grain boundaries can be significantly different from the grain interior counterparts. Since the relative phase stabilities may vary depending on the compositions, following the mechanisms discussed in section 3.1, the phases near grain boundaries would behave differently from those of the grain interior. If the segregation of α-stabilizer is induced at a grain boundary, the heterogeneous nucleation of α phase can be easily induced at the grain boundary owing to the chemically and/or elastically reduced nucleation barrier. Subsequently, the formation of GB-α phase may perturb the solute distribution nearby and initiate further α phase nucleation to form α colonies. To qualitatively investigate the effects of solute-GB interactions on the transformation kinetic pathways, the following additional solute-GB interaction potential[51] can be incorporated into the Gibbs free energy function (Eq 3):

$$f^{\text{sol-GB}} = -w^g \cdot g(\{\phi_g\}) \cdot (m_{\text{Al}} \cdot X_{\text{Al}} + m_{\text{V}} \cdot X_{\text{V}}), \quad \text{(Eq 8)}$$

where w^g is the barrier height, $\{\phi_g\}$ are grain order parameters describing the grain structure, $g(\{\phi_g\})$ is the Landau-type energy function associated with the topological features of the solute-grain boundary interaction potential, m_{Al} and m_{V} represent the interaction strength of Al and V with GBs, respectively. The solute distribution near GBs can be determined with the additional energetic contribution in Eq 8, and the possible kinetic pathway can be analyzed by applying the theoretical framework described in this work.

4.3 Limitation of the Current Framework

First of all, our current framework largely relies on the bulk thermodynamics of given phases ignoring the possible effects of interphase boundaries The kinetic pathways due to structural inhomogeneities (as discussed in section 4.2), and the details of the transformation kinetics (e.g., the details of nucleation and growth kinetics) can only be qualitatively understood. In fact, the interfacial energy and coherency strain energy arising from the presence of interfaces between different phases can alter the phase stabilities and transformation kinetics. To investigate these effects, we may employ the gradient thermodynamic approach based on the diffuse-interface description[52] in which interfacial energy and coherency strain energy are naturally incorporated.

In addition, our current framework excludes some metastable phases although our free energy functions are based on the realistic thermodynamic databases. For instance, the metastable ω phase can form athermally or isothermally in β-Ti alloys, which usually acts as a precursor for the formation of an incoherent α phase.[1,2] The formation of the ω phase takes place when the given alloy contain large amount of β-stabilizers. In Ti-6Al-4V, although the ω phase is not frequently observed[1] due to the limited amount of β-stabilizers, certain specific processing conditions (e.g., upon rapid solidification as reported in[53]) can lead to the formation of the ω phase by inducing large fluctuations of local compositions of alloying elements. Since the reliable thermodynamic description of the

ω phase is currently unavailable to our knowledge, we exclude this phase for our analysis.

In spite of the above limitations, we emphasize that our theoretical framework is quite general and the fundamental characteristics of the identified kinetic pathways would not be significantly altered by the above-mentioned additional contributions.

5. Summary

In this study, we extended the phase transformation kinetic pathway analysis by Heo et al.[20] to multi-component Ti alloys. Using a ternary Ti-6Al-4V as a model system, we demonstrated how the realistic thermodynamic database is incorporated into the graphical thermodynamic framework and predicted the possible transformation pathways under different thermal treatment conditions. Several possible pathways involving the complicated coupling between diffusional and diffusionless processes were verified for the isothermal heat treatment condition. For the non-isothermal conditions, we discussed the effects of cooling rates (or the degree of undercooling) in the light of phase stability analysis. The possible extension to general multi-component alloys was also discussed to consider the effects of multiple minor alloying elements on the kinetic pathways. In addition to the conventional pathways, we briefly discussed the possible extension of our framework to the so-called non-conventional kinetic pathways. We emphasize that the theoretical analysis of the possible kinetic pathways based on the graphical thermodynamic approach is able to help understand the key features of phase transformation mechanisms in generic multi-component Ti alloys.

References

1. R. Boyer, E.W. Collings, and G. Welsch, *Material Properties Handbook: Titanium Alloys*, ASM International, Metals Park, 1994
2. G. Lütjering and J.C. Williams, *Titanium*, 2nd ed., Springer, Berlin, 2007
3. S. Malinov, Z. Guo, W. Sha, and A. Wilson, Differential Scanning Calorimetry Study and Computer Modeling of β ⇒ α Phase Transformation in a Ti-6Al-4V Alloy, *Metall. Mater. Trans. A*, 2001, **32A**, p 879

4. W. Petry, A. Heiming, J. Trampenau, M. Alba, C. Herzig, H.R. Schober, and G. Vogl, Phonon Dispersion of the bcc Phase of Group-IV Metals. I. bcc Titanium, *Phys. Rev. B*, 1991, **43**, p 10933-10947

5. G. Lütjering, Influence of Processing on Microstructure and Mechanical Properties of (α + β) Titanium Alloys, *Mater. Sci. Eng. A*, 1998, **243**, p 32-45

6. S. Nag, Y. Zheng, R.E.A. Williams, A. Devaraj, A. Boyne, Y. Wang, P.C. Collins, G.B. Viswanathan, J.S. Tiley, B.C. Muddle, R. Banerjee, and H.L. Fraser, Non-Classical Homogeneous Precipitation Mediated by Compositional Fluctuations in Titanium Alloys, *Acta Mater.*, 2012, **60**, p 6247-6256

7. C.G. Rhodes and J.C. Williams, The Precipitation of α-Phase in β-Phase Ti Alloys, *Metall. Trans. A*, 1975, **6A**, p 2103

8. E.S.K. Menon and R. Krishnan, Phase Transformations in Ti-V Alloys Part 2 α and ω Formation, *J. Mater. Sci.*, 1983, **18**, p 365-374

9. E.S.K. Menon and R. Krishnan, Phase Transformations in Ti-V Alloys Part 1 Martensitic Transformations, *J. Mater. Sci.*, 1983, **18**, p 375-382

10. S.M.C. van Bohemen, J. Sietsma, and S. van der Zwaag, Experimental Observations Elucidating the Mechanisms of Structural bcc-hcp Transformations in β-Ti Alloys, *Phys. Rev. B*, 2006, **74**, p 134114

11. N. Stanford and P.S. Bate, Crystallographic Variant Selection in Ti-6Al-4V, *Acta Mater.*, 2004, **52**, p 5215-5224

12. T. Ahmed and H.J. Rack, Phase Transformations During Cooling in α + β Titanium Alloys, *Mater. Sci. Eng. A*, 1998, **243**, p 206-211

13. W.A. Soffa and D.E. Laughlin, Decomposition and Ordering Processes Involving Thermodynamically First-Order Order → Disorder Transformations, *Acta Metall.*, 1989, **37**, p 3019-3028

14. A.G. Khachaturyan, T.F. Lindsey, and J.J.W. Morris, Theoretical Investigation of the Precipitation of δ' in Al-Li, *Metall. Mater. Trans. A*, 1988, **19A**, p 249

15. D.N. Fan and L.-Q. Chen, Possibility of Spinodal Decomposition in ZrO$_2$-Y$_2$O$_3$ Alloys: A Theoretical Investigation, *J. Am. Ceram. Soc.*, 1995, **78**, p 1680-1686

16. Y. Ni, Y.M. Jin, and A.G. Khachaturyan, The Transformation Sequences in the Cubic → Tetragonal Decomposition, *Acta Mater.*, 2007, **55**, p 4903-4914

17. Y. Ni and A.G. Khachaturyan, From Chessboard Tweed to Chessboard Nanowire Structure during Pseudospinodal Decomposition, *Nat. Mater.*, 2009, **8**, p 410

18. R.B. Gullberg, R. Taggart, and D.H. Polonis, On the Decomposition of the Beta Phase in Titanium Alloys, *J. Mater. Sci.*, 1971, **6**, p 384-389

19. M.K. Koul and J.F. Breedis, Phase Transformations in Beta Isomorphous Titanium Alloys, *Acta Metall.*, 1970, **18**, p 579

20. T.W. Heo, D.S. Shih, and L.-Q. Chen, Kinetic Pathways of Phase Transformations in Two-Phase Ti Alloys, *Metall. Mater. Trans. A*, 2014, **45**, p 3438-3445

21. A. Boyne, D. Wang, R.P. Shi, Y. Zheng, A. Behera, S. Nag, J.S. Tiley, H.L. Fraser, R. Banerjee, and Y. Wang, Pseudospinodal Mechanism for Fine α/β Microstructures in β-Ti Alloys, *Acta Mater.*, 2014, **64**, p 188-197

22. D. Wang, R. Shi, Y. Zheng, R. Banerjee, H.L. Fraser, and Y. Wang, Integrated Computational Materials Engineering (ICME) Approach to Design of Novel Microstructures for Ti-Alloys, *JOM*, 2014, **66**, p 1287-1298

23. G.B. McFadden, A.A. Wheeler, R.J. Braun, S.R. Coriell, and R.F. Sekerka, Phase-Field Models for Anisotropic Interfaces, *Phys. Rev. E*, 1993, **48**, p 2016-2024

24. S.-L. Wang, R.F. Sekerka, A.A. Wheeler, B.T. Murray, S.R. Coriell, R.J. Braun, and G.B. McFadden, Thermodynamically-Consistent Phase-Field Models for Solidification, *Physica D*, 1993, **69**, p 189-200

25. A.G. Khachaturyan, *Theory of Structural Transformations in Solids*, Wiley, New York, 1983

26. F. Zhang, Personal Communication, CompuTherm LLC, Madison, WI, 2013

27. F. Zhang, S.L. Chen, Y.A. Chang, N. Ma, and Y. Wang, Development of Thermodynamic Description of a Pseudo-Ternary System for Multicomponent Ti64 Alloy, *J. Phase Equilib. Diffus.*, 2007, **28**, p 115-120

28. W.G. Burgers, On the Process of Transition of the Cubic-Body-Centered Modification into the Hexagonal-Close-Packed Modification of Zirconium, *Physica*, 1934, **1**, p 561-586

29. S.G. Kim, W.T. Kim, and T. Suzuki, Phase-Field Model for Binary Alloys, *Phys. Rev. E*, 1999, **60**, p 7186

30. L.-Q. Chen, Computer Simulation of Spinodal Decomposition in Ternary Systems, *Acta Metall. Mater.*, 1994, **42**, p 3503

31. H.I. Aaronson and J.K. Lee, *Lectures on the Theory of Phase Transformations*, TMS, New York, 1975

32. D. Qiu, R. Shi, D. Zhang, W. Lu, and Y. Wang, Variant Selection by Dislocations during α Precipitation in α/β Titanium Alloys, *Acta Mater.*, 2015, **88**, p 218-231

33. Y. Ohmori, K. Nakai, H. Ohtsubo, and M. Tsunofuri, Formation of Widmanstätten Alpha Structure in a Ti-6Al-4V Alloy, *Mater. Trans. JIM*, 1994, **35**, p 238-246

34. G. Welsch, G. Lütjering, K. Gazioglu, and W. Bunk, Deformation Characteristics of Age Hardened Ti-6Al-4V, *Metall. Trans. A*, 1977, **8A**, p 169

35. T.M. Radchenko, V.A. Tatarenko, and H. Zapolsky, Statistical Thermodynamics and Ordering Kinetics of DO$_{19}$-type Phase: Application of the Models for HCP Ti-Al Alloy, *Solid State Phenom.*, 2008, **138**, p 283-302

36. R.G. Hennig, T.J. Lenosky, D.R. Trinkle, S.P. Rudin, and J.W. Wilkins, Classical Potential Describes Martensitic Phase Transformations between the α, β, and ω Titanium Phases, *Phys. Rev. B*, 2008, **78**, p 054121

37. M. Sanati, A. Saxena, T. Lookman, and R.C. Albers, Landau Free Energy for a bcc-hcp Reconstructive Phase Transformation, *Phys. Rev. B*, 2001, **63**, p 224114

38. S. Malinov, W. Sha, and Z. Guo, Application of Artificial Neural Network for Prediction of Time-Temperature-Transformation Diagrams in Titanium Alloys, *Mater. Sci. Eng. A*, 2000, **283**, p 1-10

39. P. Tarín, F.X. Gil, M.P. Ginebra, J.M. Manero, J.M. Prado, M. Solé, and J.A. Planell, Structural Transformations in Ti-6Al-4V Alloy, *J. Phys. IV*, 1995, **05**, p C2-317-C312-322

40. M. Yan and P. Yu, An Overview of Densification, Microstructure and Mechanical Property of Additively Manufactured Ti-6Al-4V—Comparison among Selective Laser Melting, Electron Beam Melting, Laser Metal Deposition and Selective Laser Sintering, and with Conventional Powder, *Sintering Techniques of Materials*, A. Lakshmanan, Ed., InTech, Rijeka, 2015,

41. R. Dąbrowski, The Kinetics of Phase Transformations During Continuous Cooling of the Ti-6Al-4V Alloy from the Single-Phase β Range, *Arch. Metall. Mater.*, 2011, **56**, p 703-707

42. J. Sieniawski, W. Ziaja, K. Kubiak, and M. Motyk, Microstructure and Mechanical Properties of High Strength Two-Phase Titanium Alloys, *Titanium Alloys—Advances in Properties Control*, J. Sieniawski and W. Ziaja, Ed., InTech, Rijeka, 2013,

43. J.I. Qazi, O.N. Senkov, J. Rahim, and F.H. Froes, Kinetics of Martensite Decomposition in Ti-6Al-4V-xH Alloys, *Mater. Sci. Eng. A*, 2003, **359**, p 137-149

44. L. Kaufman, Computational Thermodynamics and Materials Design, *CALPHAD*, 2001, **25**, p 141-161
45. D.M. Cupid, M.J. Kriegel, O. Fabrichnaya, F. Ebrahimi, and H.J. Seifert, Thermodynamic Assessment of the Cr-Ti and First Assessment of the Al-Cr-Ti Systems, *Intermetallics*, 2011, **19**, p 1222-1235
46. U.R. Kattner and W.J. Boettinger, Thermodynamic Calculation of the Ternary Ti-Al-Nb System, *Mater. Sci. Eng. A*, 1992, **A152**, p 9-17
47. H. Wang, N. Warnken, and R.C. Reed, Thermodynamic and Kinetic Modeling of bcc Phase in the Ti-Al-V Ternary System, *Mater. Sci. Eng. A*, 2010, **528**, p 622-630
48. V.T. Witusiewicz, A.A. Bondar, U. Hecht, V.M. Voblikov, O.S. Fomichov, V.M. Petyukh, and S. Rex, Experimental Study and Thermodynamic Modelling of the Ternary Al-Ta-Ti System, *Intermetallics*, 2011, **19**, p 234-259
49. X.G. Lu, C.H. Li, L.Y. Chen, A.T. Qiu, and W.Z. Ding, Calculation of Phase Equilibria in Ti-Al-Cr-Mn Quaternary System for Developing Lower Cost Titanium Alloys, *Mater. Chem. Phys.*, 2011, **129**, p 718-728
50. H. Wang, N. Warnken, and R.C. Reed, Thermodynamic Assessment of the Ordered B2 Phase in the Ti-V-Cr-Al Quaternary System, *CALPHAD*, 2011, **35**, p 204-208
51. T.W. Heo, S. Bhattacharyya, and L.-Q. Chen, A Phase-Field Study of Strain Energy Effects on Solute-Grain Boundary Interactions, *Acta Mater.*, 2011, **59**, p 7800-7815
52. L.-Q. Chen, Phase-Field Models for Microstructure Evolution, *Annu. Rev. Mater. Res.*, 2002, **32**, p 113-140
53. Z. Fan and A.P. Miodownik, TEM Study of Metastable β-Phase Decomposition in Rapidly Solidified Ti-6Al-4V Alloy, *J. Mater. Sci.*, 1994, **29**, p 6403-6412